

## ARTICLE OPEN



# Local mechanisms for global daytime, nighttime, and compound heatwaves

Sijia Wu<sup>1</sup>, Ming Luo<sup>1,2</sup>✉, Rui Zhao<sup>3</sup>, Jing Li<sup>4</sup>, Peng Sun<sup>5</sup>, Zhen Liu<sup>6,7</sup>, Xiaoyu Wang<sup>1</sup>, Peng Wang<sup>1</sup> and Hui Zhang<sup>1</sup>

Heatwaves impose serious impacts on ecosystems, human health, agriculture, and energy consumption. Previous studies have classified heatwaves into independent daytime, independent nighttime, and compound daytime-nighttime types, and examined the long-term changes in the three types. However, the underlying mechanisms associated with the variations in different heatwave types remain poorly understood. Here we present the first investigation of the local physical processes associated with the daytime, nighttime, and compound heatwaves over the global land during 1979–2020. The results show that three heatwave types occur frequently and increasingly in most regions worldwide. Nighttime and compound heatwaves exhibit stronger increases in both frequency (the yearly number of the events) and fraction (the ratio of the yearly number of one heatwave type to the total yearly number of all types) than daytime heatwaves. Composite diagnostic analyses of local meteorological variables suggest that daytime heatwaves are associated with increased solar radiation under dry conditions and reduced cloud cover and humidity under a clear sky. In contrast, nighttime heatwaves are typically accompanied by moist conditions with increases in cloud fraction, humidity, and longwave radiation at night. These synoptic conditions for daytime and nighttime heatwaves are combined to contribute to compound heatwaves. Local divergences and moisture fluxes responsible for different heatwaves are further revealed. Positive moisture divergence anomalies are seen in most land areas for daytime and compound heatwaves, while they mainly appear in low latitudes for nighttime heatwaves. Our research provides a comprehensive understanding of the local mechanisms of different heatwave types, informing future risks and impact assessments.

*npj Climate and Atmospheric Science* (2023)6:36; <https://doi.org/10.1038/s41612-023-00365-8>

## INTRODUCTION

Heatwave hazards are prolonged extremely hot weather events that can severely damage the environment, human health, and socioeconomic development<sup>1–4</sup>. For example, the severe European heatwave in 2003 caused over 70,000 deaths and enormous losses in agricultural production<sup>5</sup>. The 2010 Russian heatwave accompanied by drought conditions and forest fires resulted in 54,000 deaths<sup>6,7</sup>. It was observed that heatwaves have intensified over the past decades, in terms of their magnitude, frequency, and duration<sup>8,9</sup>. Under global warming, heatwave events are projected to be further exacerbated and may produce more harmful consequences on human society<sup>10,11</sup>. Heatwave events have attracted much attention from the public and scientists, and have become an essential research topic in recent years<sup>12–14</sup>. For example, Perkins-Kirkpatrick and Gibson<sup>15</sup> concluded that heatwave duration is projected to increase by 2–10 days per degree celsius, with larger changes over lower latitudes. Recent studies by You et al.<sup>16,17</sup> based on multiple definitions reported substantial increases in heatwave activities and extreme temperatures in China over the past decades. Luo et al.<sup>18</sup> found that heatwaves in arid Northwest China exhibit significant intensifying trends in terms of increasing frequency, prolonging duration, and strengthening intensity.

The characteristics of heatwaves explored by previous studies are mainly based solely on daytime maximum temperature ( $T_{\max}$ )<sup>18–20</sup>. While nighttime heatwaves characterized by a high daily minimum temperature ( $T_{\min}$ ) have a significant effect on

human comfort and inhibit the relief from nighttime cooling, thus possibly increasing threats to human health<sup>21–23</sup>. More hazardous conditions will emerge when extreme daytime temperatures are combined with the following warm nighttime for consecutive days (i.e., compound heatwaves)<sup>22–24</sup>. For instance, the compound heatwaves occurring in the mid-west of the United States in 1995 caused over 500 deaths in Chicago<sup>25</sup>. Moreover, synoptic conditions associated with daytime, nighttime, and compound heatwaves may differ<sup>26</sup>. It is necessary to distinguish different heatwave types and reveal the involved physical mechanisms.

Atmospheric conditions leading to daytime heatwaves have been well understood in the literature. One major factor causing daytime heatwaves is the anomalous anticyclonic circulation in the middle and upper troposphere, which generates subsidence and warm advection<sup>8,27–29</sup>. The subsidence associated with warming high-pressure anomalies prohibits cloud formation resulting in clear skies, thus enhancing the surface shortwave radiative heating and prolonging hot conditions<sup>30</sup>. For example, Luo and Lau<sup>31</sup> pointed out that heatwaves in southern China are accompanied by anomalous anticyclones and high pressure near the surface, resulting from the westward extension of the western North Pacific subtropical high (WNPSH). On the other hand, anomalous anticyclones can suppress convective activities, such that forms a drier and hotter soil environment in favor of the occurrence of heatwaves, as reported by Deng et al.<sup>32</sup>. In addition to the subsidence, extreme heat events can also be controlled by the intensity of temperature advection<sup>33,34</sup>. Previous studies also

<sup>1</sup>Guangdong Provincial Key Laboratory of Urbanization and Geo-simulation, School of Geography and Planning, Sun Yat-sen University, Guangzhou, China. <sup>2</sup>Institute of Environment, Energy and Sustainability, The Chinese University of Hong Kong, Shatin, Hong Kong SAR, China. <sup>3</sup>Fujian Key Laboratory of Severe Weather, Fujian Institute of Meteorological Sciences, Fuzhou, China. <sup>4</sup>College of Resources and Environment, Fujian Agriculture and Forestry University, Fuzhou, China. <sup>5</sup>School of Geography and Tourism, Anhui Normal University, Wuhu, China. <sup>6</sup>Center for Climate Physics, Institute for Basic Science, Busan, Republic of Korea. <sup>7</sup>Pusan National University, Busan, Republic of Korea. <sup>✉</sup>email: luom38@mail.sysu.edu.cn

demonstrated that anomalous atmospheric planetary waves play an essential role in the occurrence and evolution of heat extremes<sup>30,35–37</sup>. Teng et al.<sup>35</sup> found a pattern of anomalous Rossby waves before the occurrence of heatwaves in the US. A recent study by Luo et al.<sup>38</sup> based on a 3D perspective revealed that the moving pattern of contiguous heatwaves in northwestern China is accompanied by the progression of Rossby waves.

Compared with daytime heatwaves, there are few studies on the formation of nighttime heatwaves as well as the associated mechanisms. Gershunov et al.<sup>39</sup> indicated that the synoptic characteristics of daytime and nighttime heatwaves over California and Nevada are similar, while nighttime heatwaves are generally accompanied by the anomalously moist atmosphere, which can enhance downward longwave radiation during the night via intensified greenhouse effect<sup>40</sup>. Besides, Bumbaco et al.<sup>41</sup> found that precipitable water content exerts a more important role in nighttime heatwaves than daytime heatwaves over the Pacific Northwest of the US. Similar findings have been reported in other regions, such as the Korean Peninsula<sup>42</sup> and southern China<sup>26</sup>, where nighttime heatwaves are typically associated with enhanced cloud cover and humidity. Although growing studies have been made toward understanding the processes contributing to nighttime heatwaves at the regional scale, a comprehensive examination of their physical mechanisms on a global basis is lacking.

Furthermore, previous studies mainly focused on one type of heatwaves, and few studies investigated the processes contributing to compound heatwaves. Luo et al.<sup>26</sup> analyzed compound heatwaves in southern China and noticed that their characteristics resemble the combined atmospheric conditions (e.g., decreased convection and increased moisture) of daytime and nighttime heatwaves. Li et al.<sup>43</sup> also noted a similar favorable condition for compound heatwaves in the mid-lower reaches of the Yangtze River of China<sup>43</sup>. As suggested by Gershunov et al.<sup>39</sup>, the strong and persistent baroclinic circulation causes a stable low-level wind convergence, thus trapping a large amount of moisture and heat during nights and causing compound heatwaves over California and Nevada.

However, the processes and mechanisms driving daytime, nighttime, and compound heatwaves in different regions of the world have not been comprehended. In this study, we first identify

three types of heatwaves (i.e., independent daytime heatwaves, independent nighttime heatwaves, and compound heatwaves, see Methods) and examine the spatial distribution and long-term changes of these types. Then, we conduct a detailed comparative investigation of various local factors affecting these heatwaves at the grid cell over the global land. This examination will provide a comprehensive investigation of the local mechanisms of daytime, nighttime, and compound heatwaves, which may improve the forecast skill of extreme weather and climate events.

## RESULTS

### Spatial distribution and long-term changes of three heatwave types

We first examine the global patterns of frequency and fraction (see Methods) of summertime daytime, nighttime, and compound heatwaves during 1979–2020 (Fig. 1). It can be seen that three types of heatwaves frequently occur in most parts of the continents, with an average frequency (fraction) of 8.10 events (17.53%) for daytime, 10.85 events (24.43%) for nighttime, and 23.66 events (58.04%) for compound heatwaves. Their frequency and fraction exhibit geographical heterogeneity, with maximums for daytime and nighttime heatwaves concentrated over northeastern Asia (around 60°N) and low latitudes (30°S–30°N), such as southern America, northeastern and central Asia, northern Africa, and northern Australia. On the contrary, compound heatwaves occur more frequently at mid-to-high latitudes in the Northern Hemisphere. Besides, South America and Australia also experienced frequent compound heatwave events.

To inspect the temporal evolution of summertime daytime, nighttime, and compound heatwaves during 1979–2020, we calculate the yearly time series of annual mean frequency and fraction of each heatwave type, which is area-averaged in all land grids over a corresponding year. As shown in Fig. 2a, the frequency of all types of heatwaves has increased significantly from 1979 to 2020, with trends reaching 0.02, 0.04, and 0.06 events per decade for daytime, nighttime, and compound heatwaves, respectively. For the fraction trends, they have increased by 1.37% and 1.16% per decade for nighttime and compound heatwaves, respectively, but decreased by 2.53% per decade for daytime heatwaves (Fig. 2b). Both frequency and

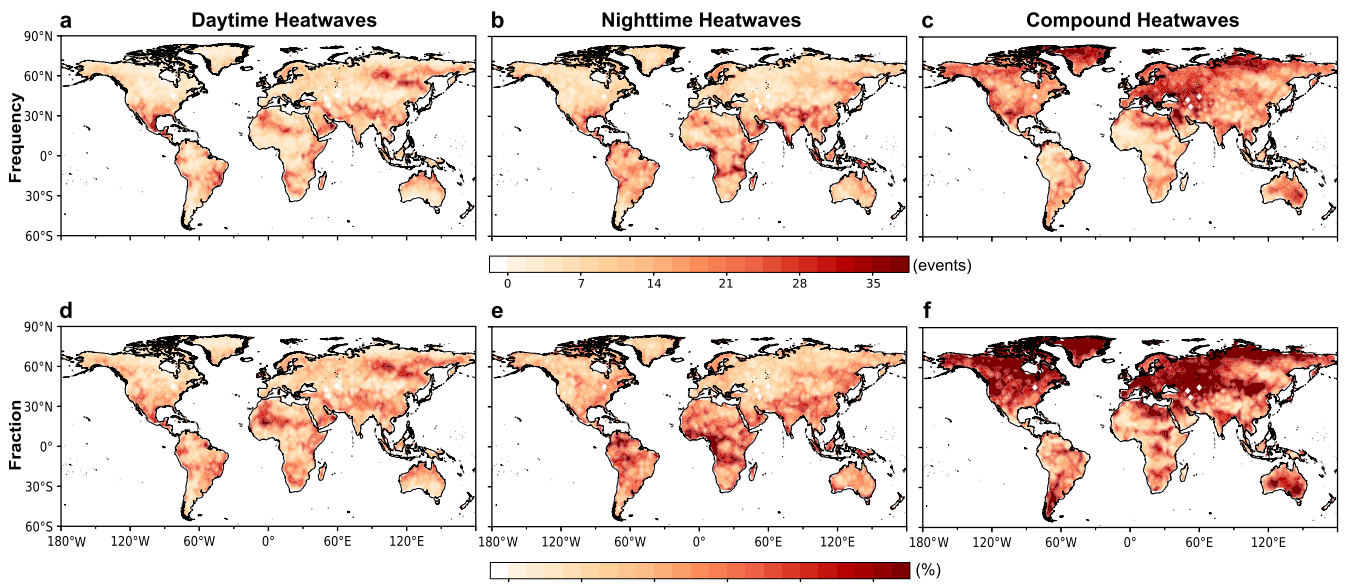
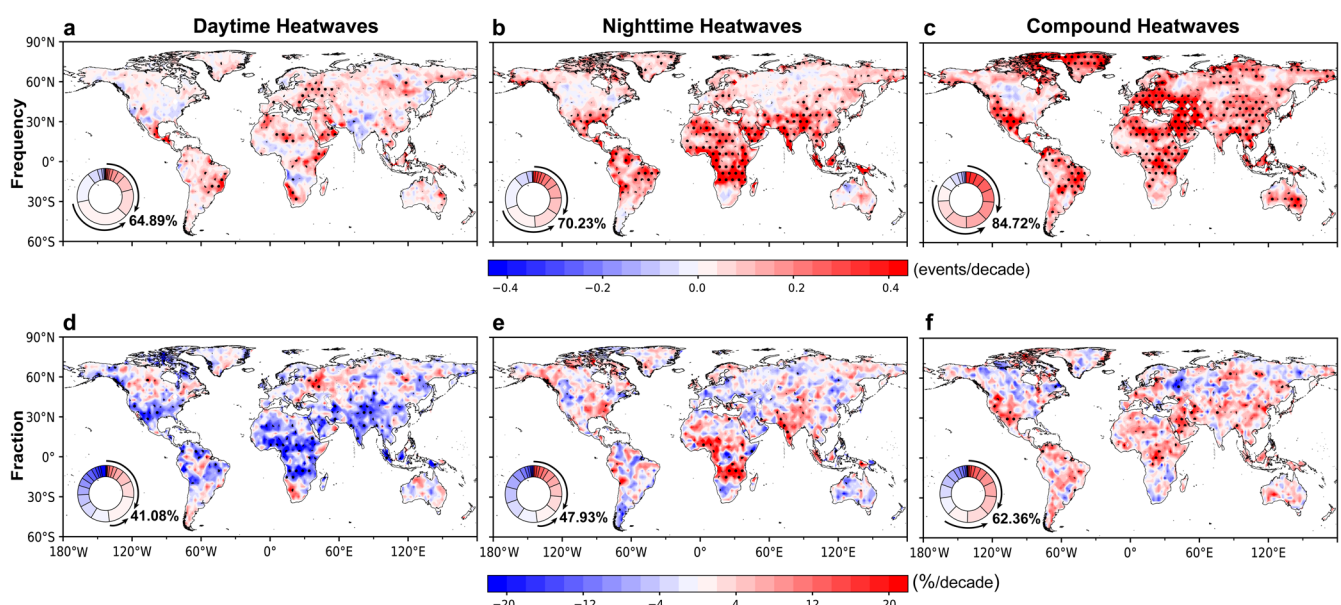
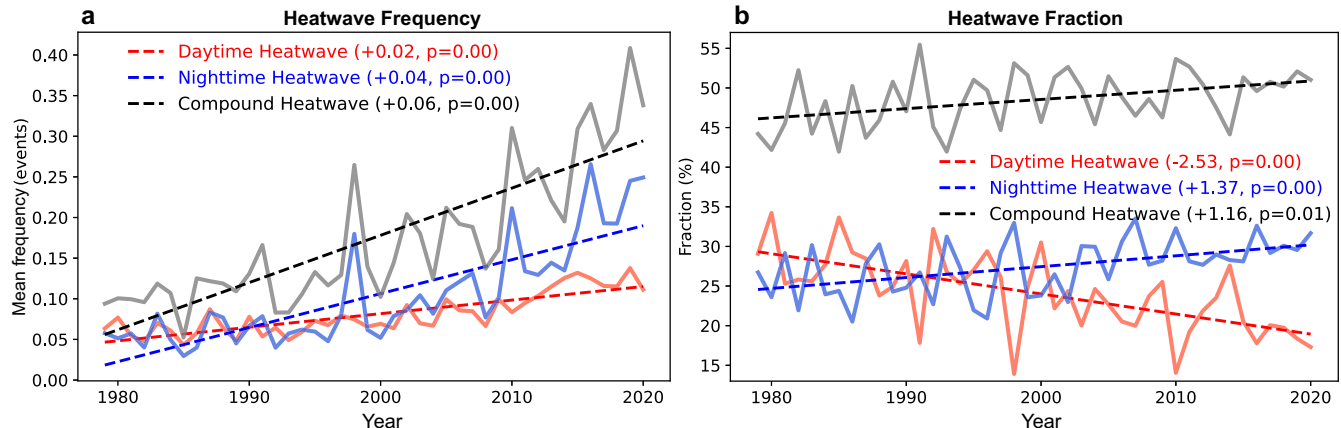


**Fig. 1 Spatial distributions of the frequency and fraction of different heatwaves.** a–c The total frequency of daytime **a**, nighttime **b**, and compound **c** heatwaves during 1979–2020. d–f The fraction in the percentage of daytime **d**, nighttime **e**, and compound **f** heatwaves during 1979–2020.



fraction changes suggest that nighttime and compound heatwaves are becoming more frequent and stronger than daytime heatwaves. It may be related to the fact that global warming in the nighttime period is stronger than during the daytime<sup>44,45</sup>. Figure 3 presents the global patterns of trends per decade in heatwave frequency and fraction. The frequency of the three types tends to increase in most global land areas, with mean trends of 0.04, 0.09, and 0.16 events per decade for summertime daytime, nighttime, and compound heatwaves, respectively. Similar patterns can be seen in the fraction of nighttime heatwaves (0.14% per decade) and compound heatwaves (1.99% per decade). However, the fraction of daytime heatwaves decreases at most low-to-middle latitudes, with a global average of 2.13% per decade. In particular, compound heatwave frequency and fraction have increased at most grids (84.72% and 62.36% of the total grids, respectively), and nearly half of the land areas exhibit upward trends of >0.2 events and 4% per decade, respectively. Moreover, noticeable increments in the frequency and fraction of independent

nighttime heatwaves are mainly observed at low-to-middle latitudes, while the frequency trends of daytime heatwaves are spatially heterogeneous.

#### Local mechanisms for three types of heatwaves

To better understand physical mechanisms contributing to different types of heatwaves, we utilize composite analysis to examine the changes in multiple atmospheric variables (i.e., 2-meter temperature and specific humidity, cloud cover, soil moisture, surface radiation, heat flux, and vertical integration of moisture fluxes) during heatwave events. More detailed information about the composite analysis can be found in Methods. Figure 4 gives positive daytime and nighttime composite maps of anomalous near-surface air temperature 2 m above the ground (T2m) during the identified daytime, nighttime, and compound heatwave events, showing prominent meridional temperature gradients with maximum warming over high latitudes, regardless

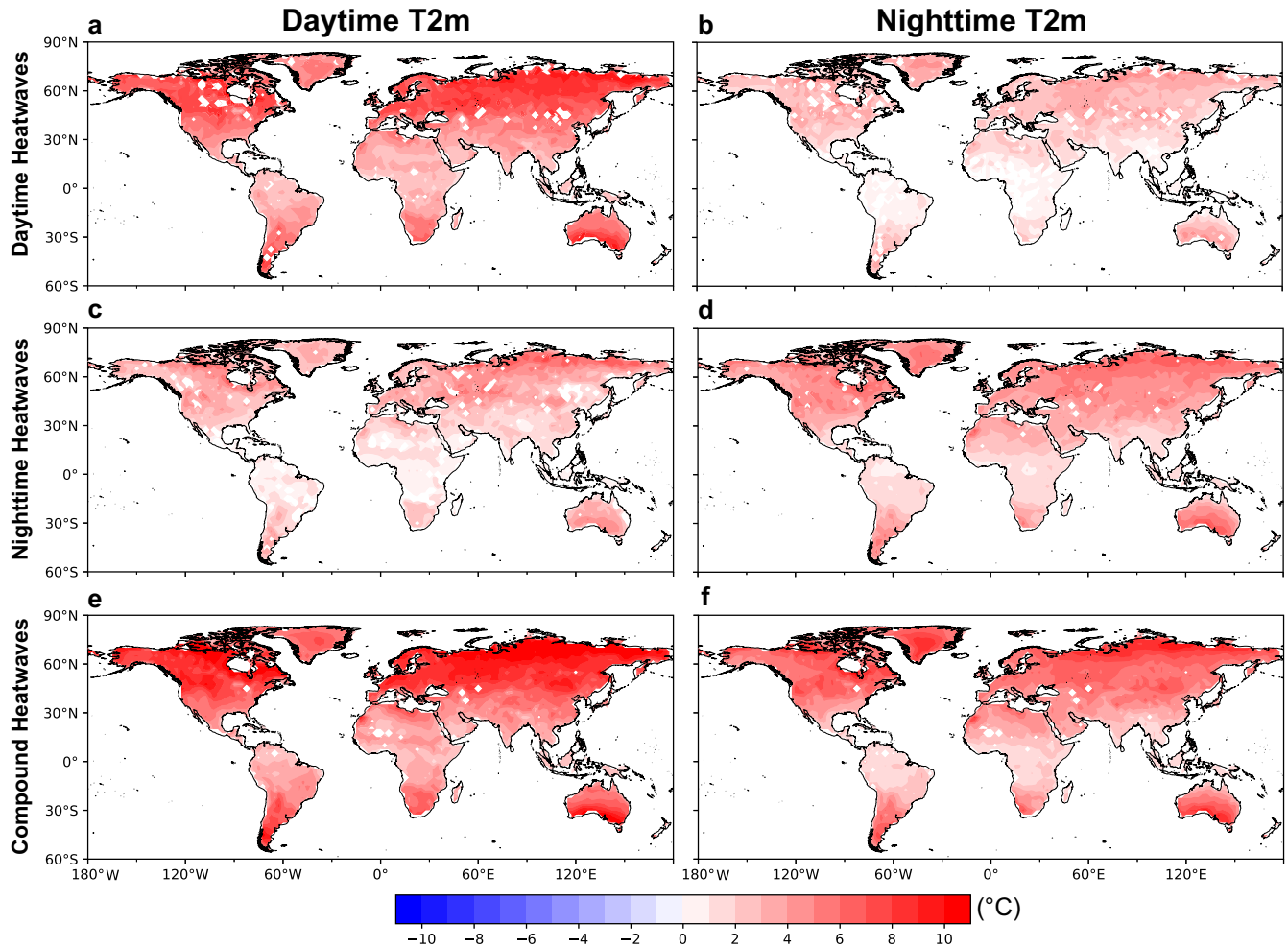


**Fig. 4 Near-surface temperature changes during different heatwaves.** **a, c, e** Composite maps of daytime near-surface air temperature (T2m) anomalies during the daytime **a**, nighttime **c**, and compound **e** heatwave events. **b, d, f** as **a, c, e** but for nighttime T2m anomalies. Daytime (nighttime) composites are computed from the data in the daytime (nighttime) hours throughout the heatwave event. Regions with the composite mean not passing the 0.05 significance level by the Student's *t*-test are masked out.

of heatwave types. It is clear that positive anomalies in T2m during daytime hours of daytime heatwave events (Fig. 4a) are stronger than the T2m anomalies during daytime hours of nighttime heatwaves (Fig. 4c). Meanwhile, the T2m anomalies during nighttime hours of nighttime heatwave events (Fig. 4d) are stronger than those during nighttime hours of daytime events (Fig. 4b). As expected, Fig. 4c (4b) shows that daytime (nighttime) T2m for nighttime (daytime) heatwaves exhibit the weakest anomalies. Compared with independent daytime (Fig. 4a, b) or nighttime (Fig. 4c, d) heatwaves, compound heatwaves (Fig. 4e, f) show the largest positive anomalies in T2m during all-time hours. Figure 5 shows the composite anomalies of total cloud cover and specific humidity during the daytime, nighttime, and all-time hours for daytime, nighttime, and compound heatwaves, respectively. Note that daytime heatwaves are associated with reduced daytime cloud cover over most parts of the global land areas (Fig. 5a). The decreased daytime cloud cover allows the surface to receive more solar shortwave radiation (see Fig. 6a), thus increasing the near-surface temperature (see Fig. 4a). Meanwhile, the reduction in daytime specific humidity is also observed in most land areas (except for the north of 50°N) (Fig. 5b), which further results in an enhancement of solar radiation to heat the air near the surface<sup>21,46</sup>. The dry and hot conditions with less cloud cover and more solar radiation provide a favorable environment for the occurrence and maintenance of daytime heatwaves<sup>47</sup>.

During preceding daytime hours of nighttime heatwaves, positive anomalies of total cloud cover are observed over coastal areas of southern South America and eastern North America, Greenland, northwestern Africa, Tibet, and eastern Eurasia, and positive specific humidity anomalies are observed over most parts of the land areas (Supplementary Fig. 1). As shown in Fig. 6, the land surface receives significantly weaker downward solar radiation during nighttime heatwaves (Fig. 6c) than daytime heatwaves (Fig. 6a). This result suggests that, unlike daytime heatwaves, nighttime heatwaves are triggered by longwave radiation rather than shortwave radiation. During nighttime hours of nighttime heatwaves, the anomalies of total cloud cover and specific humidity are also positive (Fig. 5c, d). The increased cloud cover enhances downward longwave radiation at the surface at night (Fig. 6d), warming up the air near the surface, and the increased water vapor can intensify the greenhouse effects upholding nighttime temperature<sup>39,48,49</sup>. It is consistent with previous studies explaining extreme nighttime heat over southern China<sup>26</sup>, the contiguous United States<sup>40</sup>, and the Korean Peninsula<sup>42</sup>.

It is also noted that the surface receives more solar shortwave radiation during daytime heatwaves than longwave radiation during nighttime heatwaves (see Fig. 6a, d), which can be corroborated by near-surface warming as shown in Fig. 4a, d (i.e., stronger warming in daytime T2m for daytime heatwaves than nighttime T2m for nighttime heatwaves). Compared with

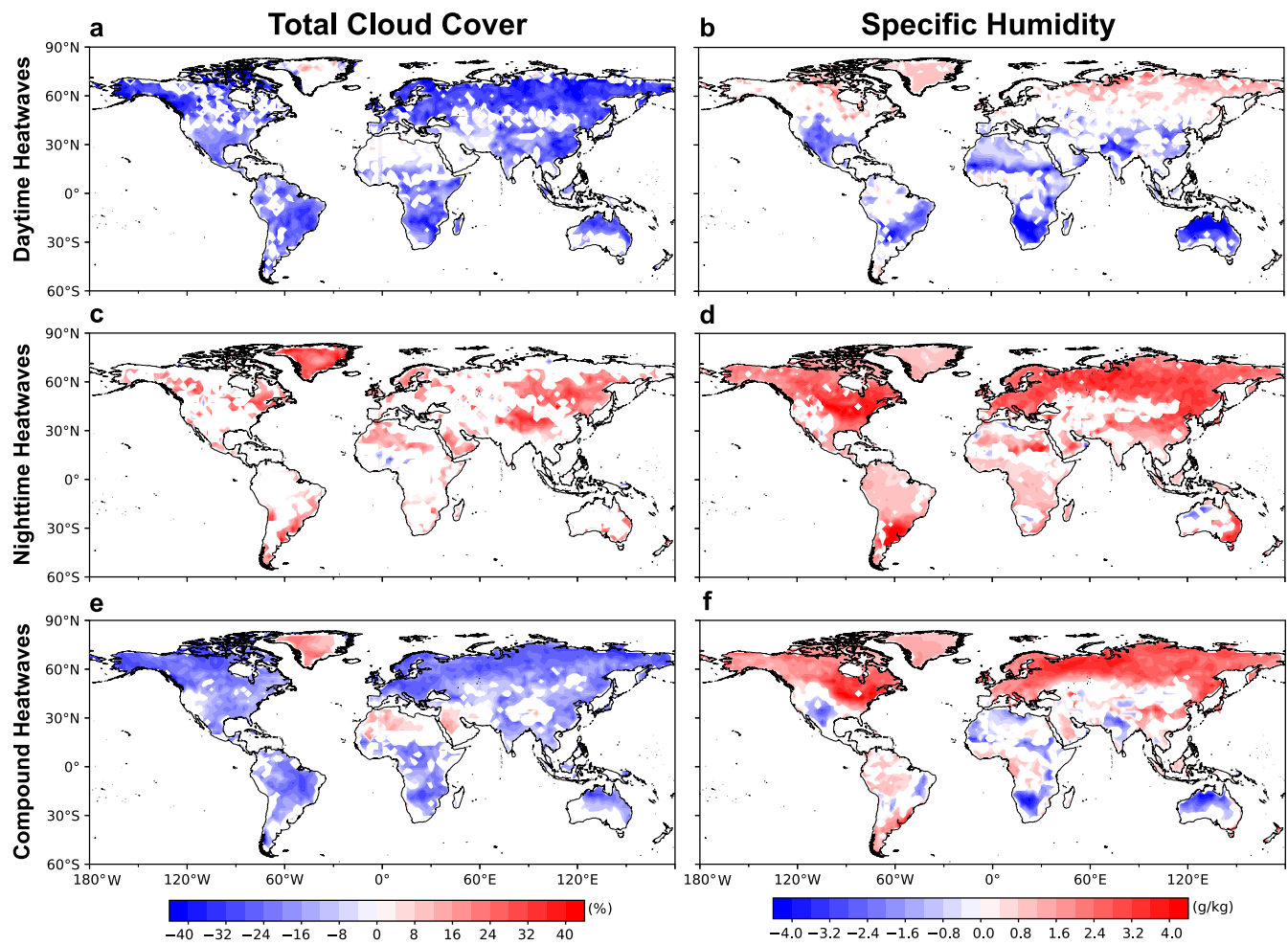


**Fig. 5 Cloud and humidity changes during different heatwaves.** **a, b** Composite maps of daytime total cloud cover and 2-meter specific humidity anomalies for daytime heatwave events. **c–f** as **a, b**, but for anomalies during the nighttime hours for nighttime heatwaves **c, d** and for anomalies during all-time hours for compound heatwaves **e, f**, respectively. Regions with the composite mean not passing the 0.05 significance level by the Student's *t*-test are masked out.

independent daytime and nighttime heatwaves, compound heatwaves are associated with stronger solar shortwave and longwave radiations (Fig. 6e, f), which collectively play an essential role in anomalously high temperatures at night and the preceding day (Fig. 4e, f).

The composite of daily precipitation and soil moisture anomalies during the daytime, nighttime, and compound heatwave events are shown in Fig. 7. Daytime and compound heatwaves are associated with negative anomalies in precipitation (Fig. 7a, e) and soil moisture (Fig. 7b, f) over entire continental regions. Soil moisture depletion leads to a reduction in evaporative cooling, which even further exacerbates the heat through land-atmosphere interactions<sup>40,50,51</sup>. This feedback could be expected to affect cloud formation, precipitation, and the daytime atmospheric boundary layer<sup>52,53</sup>. In contrast, both precipitation and soil moisture anomalies for nighttime heatwaves are much weaker, showing positive anomalies over northern China (Fig. 7c, d). These regions have heavy agriculture, suggesting that irrigation can exacerbate the processes of evapotranspiration<sup>54</sup> to induce cloudy and humid conditions at the local scale<sup>55</sup> favoring the formation of nighttime heatwaves (recall Fig. 5c, d).

Heat flux anomalies for daytime, nighttime, and compound heatwaves are displayed in Fig. 8. Since heat fluxes are small during nighttime (Supplementary Fig. 2), here we examine the

anomalies in surface latent and sensible heat fluxes during daytime hours for daytime, nighttime, and compound heatwave events. The magnitude of the latent (sensible) heat flux is proportional to the difference in specific humidity (temperature) between the surface and the overlying atmosphere<sup>56</sup>. During daytime heatwaves, the positive daytime latent heat flux anomalies and negative sensible heat flux anomalies are mainly observed in the regions of the U.S. Midwest, southern Africa, central Asia, and northern Australia. This is due to the arid and semi-arid areas with relatively drier and hotter conditions on the surface than the overlying atmosphere. The increased sensible heat flux from the surface to the atmosphere in these regions elevates near-surface temperatures, favoring the occurrence of daytime heatwaves there. Except for these regions, the spatial distributions of daytime surface latent heat flux (Fig. 8a) are consistent with soil moisture during daytime heatwave events (Fig. 7b). The decreased soil moisture induces the decreased surface latent heat flux<sup>40</sup>. For instance, the anomaly in surface latent heat flux is significantly negative (i.e., upward heat transport) at high latitudes and southern China in the Northern Hemisphere, and low latitudes in the Southern Hemisphere. The regions are covered by significant negative soil moisture anomalies (Fig. 7b), implying that the energy in these regions is largely controlled by water availability, which mostly affects evapotranspiration<sup>57</sup>. Compared with daytime heatwaves, the

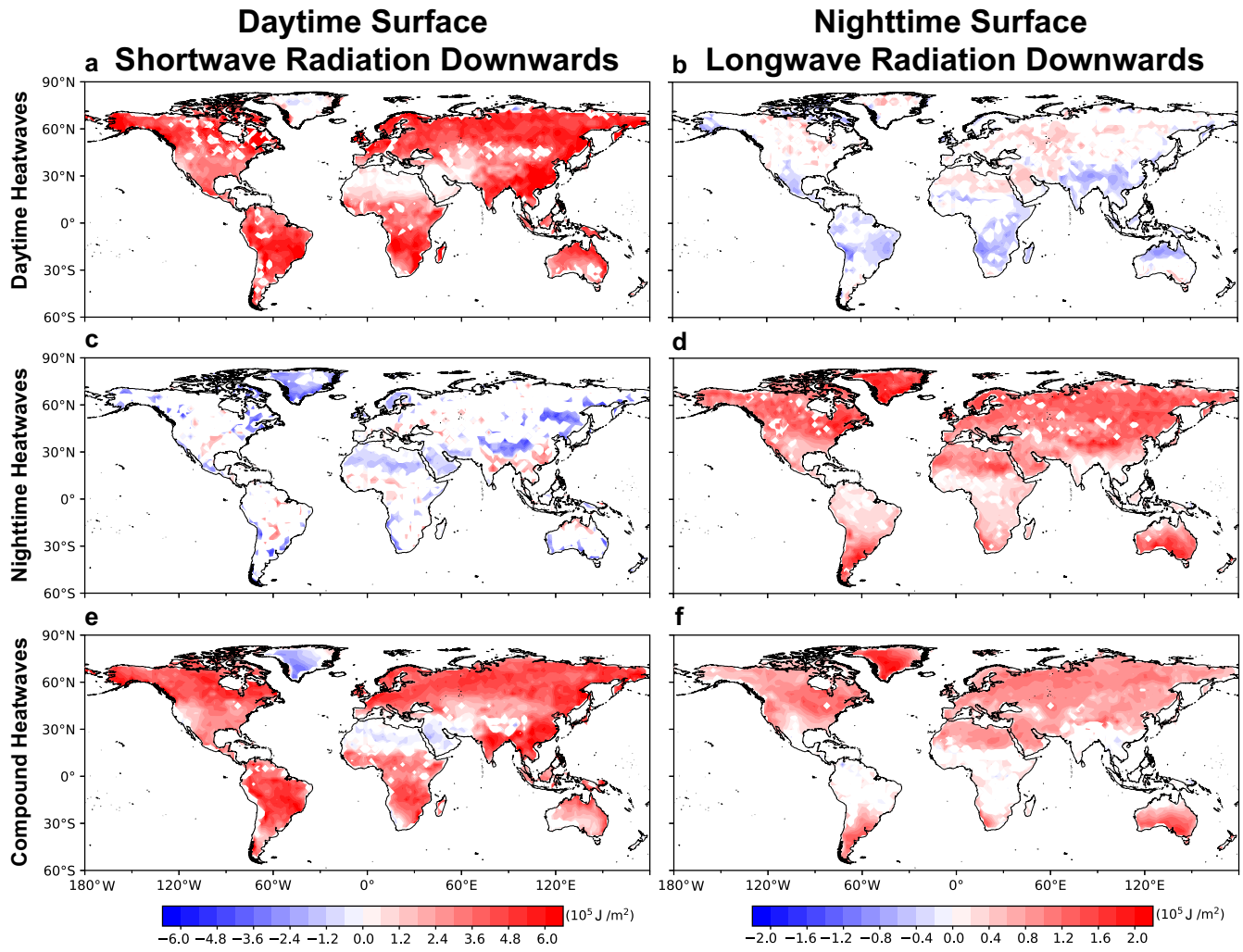


**Fig. 6 Surface radiation changes during different heatwaves. a, b** Composite maps of daytime surface shortwave radiation and nighttime surface longwave radiation anomalies for daytime heatwave events. **c–f** as **a, b**, but for anomalies for nighttime heatwaves **c, d** and compound heatwaves **e, f**, respectively. Radiation is positive downwards. Regions with the composite mean not passing the 0.05 significance level by the Student's *t*-test are masked out.

surface latent heat flux (Fig. 8c) and sensible heat flux (Fig. 8d) anomalies during nighttime heatwaves are overall less significant with smaller magnitudes. The features of combined daytime and nighttime heatwaves also appear during the daytime hours of compound heatwave events (Fig. 8e, f).

The changes in atmospheric moisture transport and divergence associated with daytime, nighttime, and compound heatwaves also reflect distinct characteristics (Fig. 9). Daytime heatwaves are associated with positive moisture divergence anomalies over most land areas (Fig. 9a). The moisture divergence and the associated downward motion form an anomalous anticyclone, which induces adiabatic warming by anomalous subsidence and enhances solar radiation by reducing humidity and cloud cover (recall Fig. 5a, b)<sup>58,59</sup>. Such warm and dry conditions with less cloud cover favor the occurrence of daytime heatwaves. The hot and dry conditions can cause potential impacts, such as wildfires, water deficit, reduction in crops, and human health risks<sup>60–62</sup>. During the nighttime heatwaves (Fig. 9b), positive moisture divergences are occurring at low latitudes and negative moisture divergence at mid-to-high latitudes. Also, southerly wind anomaly prevails over the Northern Hemisphere and northerly wind anomaly covers the Southern Hemisphere, which mainly travels from the low to high latitudes. These anomalies may result in the moisture

transporting from ocean to land areas, thus causing higher humidity and a cloudier atmosphere during nighttime heatwaves, as further verified in Fig. 5c, d. During compound heatwaves, the distribution of positive moisture divergence is alike to daytime heatwaves, which are mainly centered in northern and central South America, southern Africa, and southern and eastern Asia.

## DISCUSSION

In this study, we have classified heatwave events that occurred during the summer of 1979–2020 into the compound, independent daytime and nighttime types, and revealed the physical mechanisms contributing to each type of heatwave. The results show that three types of heatwaves increasingly occur over most parts of the world during the study period. The frequency of all heatwave types has significantly increased, while the fraction of daytime heatwaves tends to decrease, which supports the fact that the nighttime temperature rises faster than the daytime temperature<sup>63,64</sup>. Meanwhile, Karl et al.<sup>64</sup> found that the near-surface warming over the Northern Hemisphere (e.g., the contiguous United States and China) may be largely attributed to the increases in nighttime temperatures.

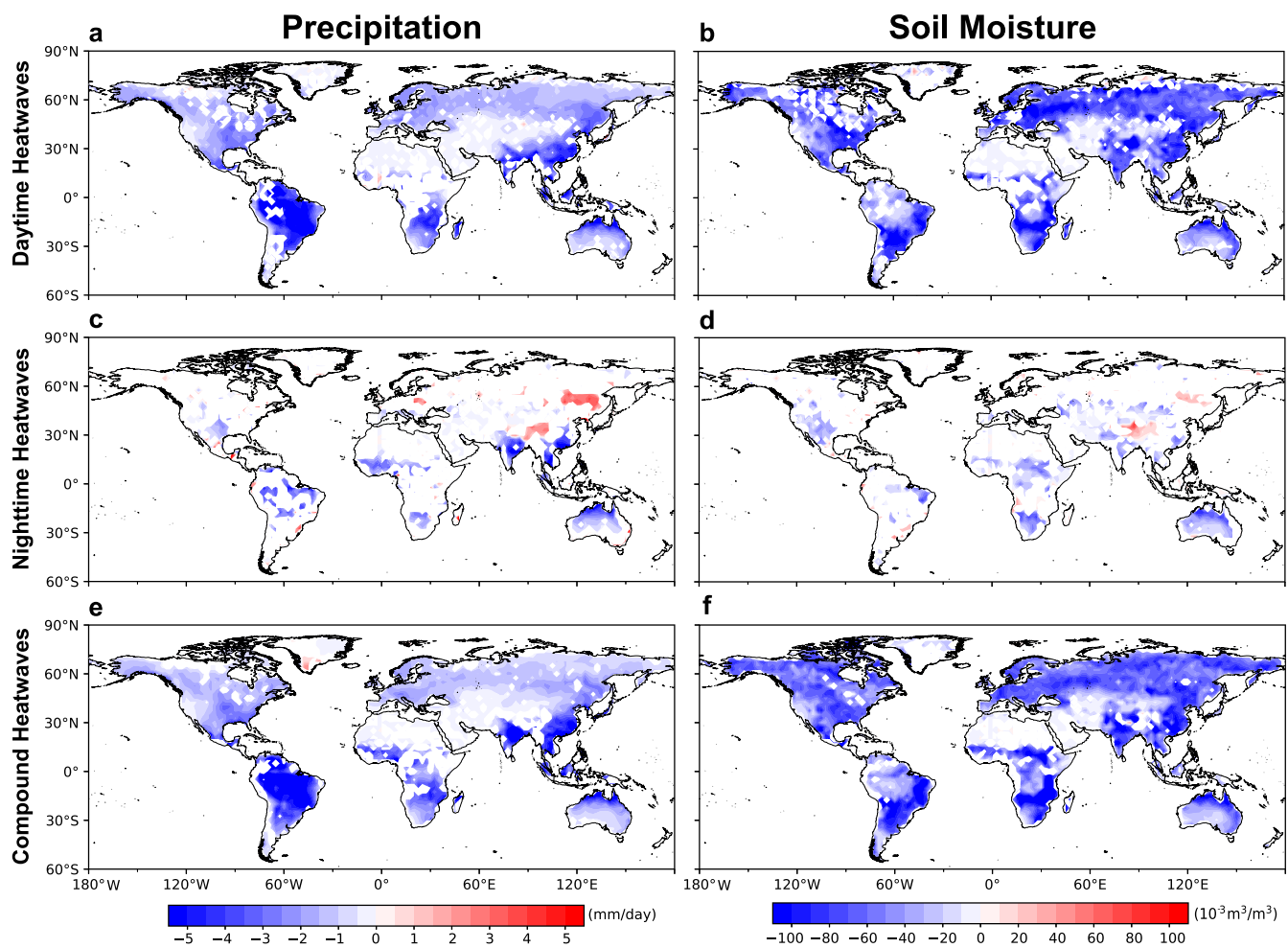


**Fig. 7 Precipitation and soil moisture changes during different heatwaves.** **a, b** Composite maps of daily precipitation and soil moisture anomalies for daytime heatwave events. **c–f** as **a, b**, but for anomalies for nighttime heatwaves **c, d** and compound heatwaves **e, f**, respectively. Regions with the composite mean not passing the 0.05 significance level by the Student's *t*-test are masked out.

Besides the above grid-based results, we also examine the changes in the frequency and fraction of daytime, nighttime, and compound heatwaves over the IPCC AR6 WGI Reference Set of Land Regions<sup>65</sup>. The regional trends are generally consistent with the gridded trends but with smaller magnitudes (Fig. 10), which are likely caused by spatial smoothing. The frequencies of three types of heatwaves exhibit robust increasing trends over almost all AR6 land regions (see left panel of Fig. 10), while the fraction trends of three heatwave types have spatial differences (see right panel of Fig. 10). In particular, the fraction of compound heatwaves displays significant increasing trends in most of the AR6 land regions, but the fraction of daytime heatwaves tends to decrease over nearly all AR6 land regions. The increasing trends in the fraction of daytime heatwaves are mainly observed in high latitudes where receive more solar radiation, thus leading to higher daytime temperatures in summer.

The occurrence of different heatwave types is controlled by distinct local conditions (Fig. 11). Our study reveals that daytime heatwaves are accompanied by increases in solar radiation, and reductions in precipitation, soil moisture, specific humidity, and cloud cover. While for nighttime heatwaves, the atmosphere becomes wetter and cloudier, which leads to more emission of longwave radiation to the surface at night, thus elevating the nighttime temperatures and favoring the occurrence of nighttime heatwaves. All these meteorological conditions are responsible for the occurrence of compound heatwaves. The physical processes

associated with different types of heatwaves are generally consistent with previous studies on heatwaves in the US<sup>40</sup> and Korea<sup>66</sup>. Besides, Luo et al.<sup>26</sup> found that daytime, nighttime, and compound heatwaves in southern China are associated with different directional extensions of both South Asian high (SAH) and WNPSH. It is noted that the existing studies related to the physical processes associated with heatwaves focused on a certain region, yet the local mechanisms contributing to different heatwave types on a global basis remain unclear.

Previous studies have also found that dynamic (or atmospheric circulation) processes are an important trigger for the occurrence of heatwaves. For example, the heatwaves in East China are associated with an enhanced WNPSH<sup>67</sup>, while those events in arid northwestern China are often accompanied by the eastward-propagating atmospheric blocking over the mid-latitudes<sup>18</sup>. The heatwaves development over central-eastern China is linked with northwesterly due to the low pressure, which can cause more heat convergence<sup>68</sup>. The extreme summer temperatures in the East Mediterranean are mostly regulated by the negative temperature advection rather than the prevailing subsidence<sup>33</sup>. It is noted that these studies mainly examined the processes associated with daytime heatwaves (i.e., defined by daily maximum temperature), while these processes associated with nighttime heatwaves are much less understood. To substantiate our interpretation of the anticyclone-surface radiation-fluxes-cloudiness feedback, we select southern China as an example to examine the dynamic

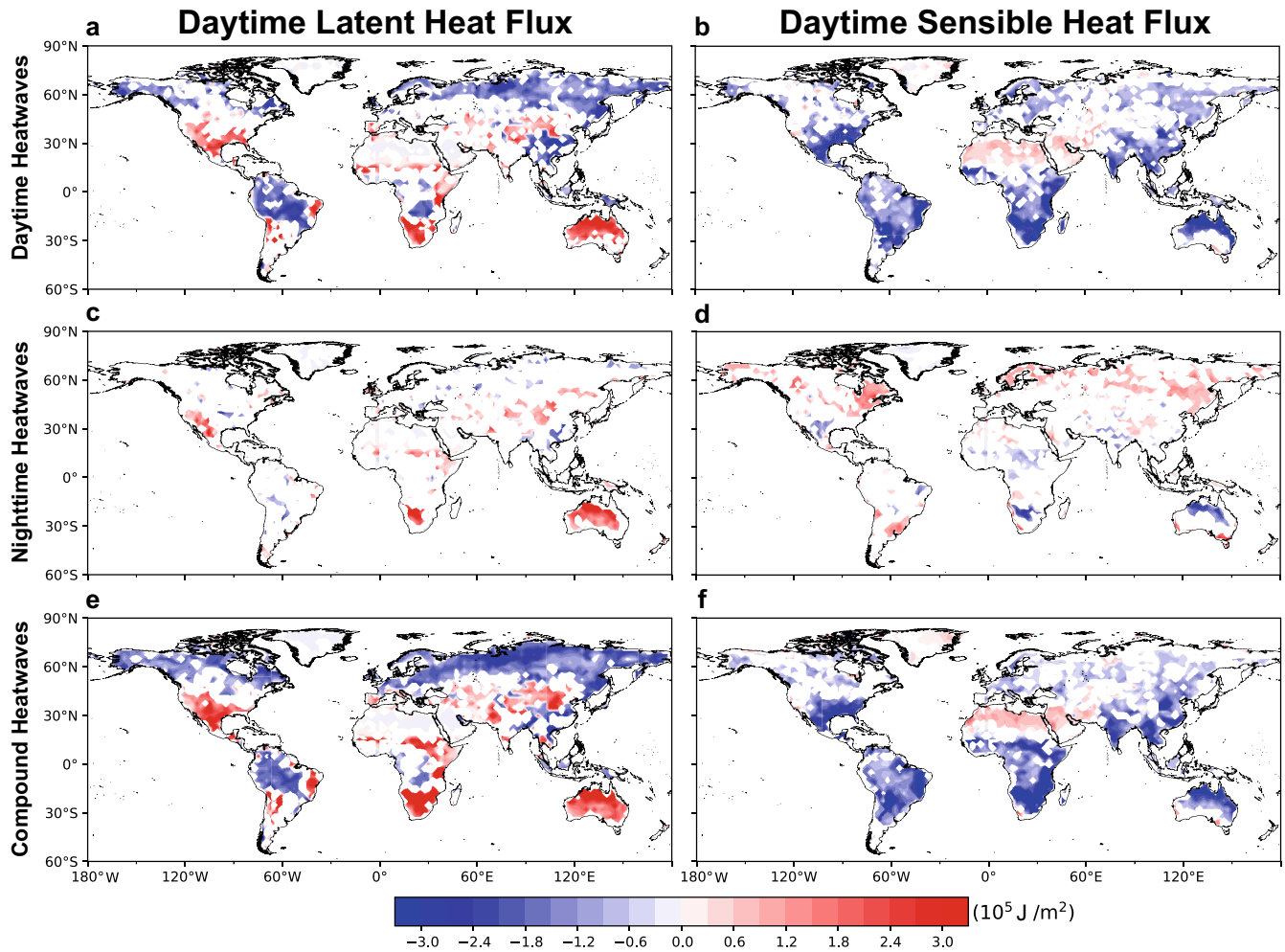


**Fig. 8 Surface heat flux changes during different heatwaves. a, b** Composite maps of daytime surface latent heat flux and surface sensible heat flux anomalies for daytime heatwave events. **c–f** as **a, b**, but for anomalies for nighttime heatwaves **c, d** and compound heatwaves **e, f**, respectively. Heat flux is positive downwards. Regions with the composite mean not passing the 0.05 significance level by the Student's *t*-test are masked out.

processes of daytime, nighttime, and compound heatwaves. The anomaly composite analyses are applied to geopotential height and horizontal wind vector at lower (850 hPa) and upper (250 hPa) troposphere, and total cloud cover, specific humidity, surface radiation, and heat flux associated with three heatwave types in southern China (Supplementary Figs. 3–6). To focus on the dynamic processes rather than the effects of long-term changes, the linear trends are removed from these atmospheric anomalies before the computation of these composites. During daytime (or compound) heatwaves, the subsidence anomaly associated with anomalous anticyclone can not only enhance the air temperature by adiabatic heating (Supplementary Fig. 3b, f), but also can decrease clouds (Supplementary Fig. 4a, e) and increase surface solar radiation (Supplementary Fig. 5a, e). Comparatively, nighttime heatwaves are accompanied by a much weaker and more southward-located high-pressure center and anticyclone anomalies over southern China (Supplementary Fig. 3d). As a result, southeastern China is prevailed by dominant southwesterly wind anomalies, which transport more water vapor to the study region and result in more clouds and moisture there (see Supplementary Fig. 4c, d). The more cloudy and humid atmosphere traps more outgoing longwave radiation and re-emits it to the surface at night (see Supplementary Fig. 5d), thus heating air temperature near the surface and contributing to nighttime heatwaves there. It is also of great interest to examine the specific atmospheric

circulation changes associated with daytime versus nighttime heatwaves in other parts of the world.

Additionally, heatwaves can also be influenced by remote factors, such as sea surface temperature (SST) anomalies, Rossby wave trains, and Arctic Sea ice extent<sup>69–71</sup>. For example, the loss of Arctic Sea ice slows down the propagation of Rossby waves in the upper-level troposphere and descending motions in the mid-latitudes, which contributes to more persistent weather conditions that are responsible for the increasing heat extremes in the Northern Hemisphere<sup>72</sup>. At the interannual scale, El Niño-Southern Oscillation (ENSO) often influences heatwave events through regulating atmospheric circulations<sup>73</sup>. For instance, anomalous SST warming during El Niño can induce sinking motion over the western North Pacific, which suppresses precipitation and condensational heating, thus intensifying heatwave activities in southern China<sup>74</sup>. In comparison, the opposite polarity in the linkage between heatwaves and La Niña tends to weaken the activities of heatwaves in these regions<sup>74</sup>. However, these previous studies have only focused on daytime heatwaves which call for research into the teleconnected effects of ENSO on nighttime heatwaves and compound heatwaves. It is also worthwhile to assess the difference between these potential factors affecting daytime, nighttime, and compound heatwaves with the use of observations and climate models.

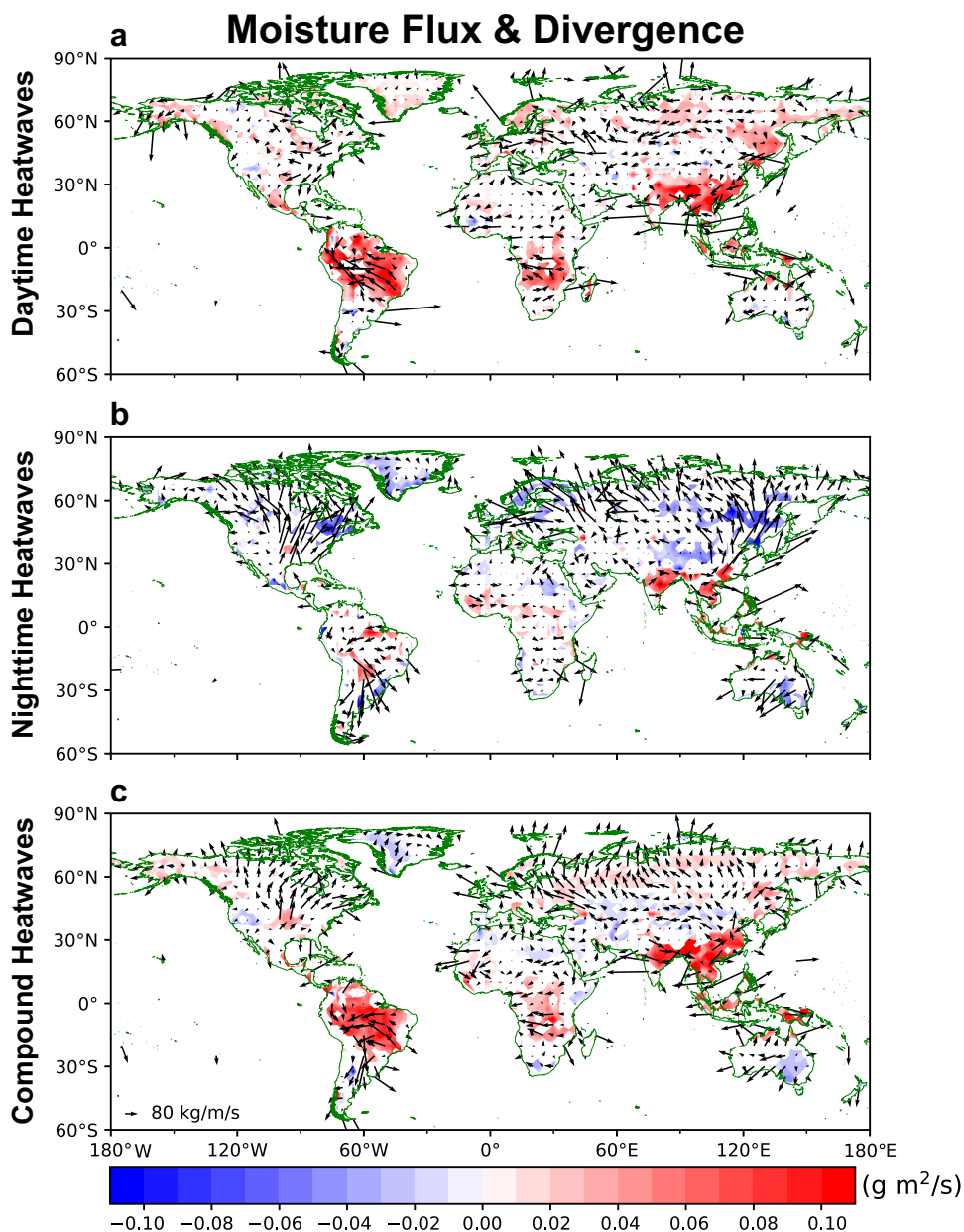


**Fig. 9** Moisture flux and divergence changes during different heatwaves. **a** Composite map of the daily vertical integral of moisture flux (vector) and divergence (shading) anomalies from the surface of the earth to the top of the troposphere for daytime heatwave events. **b, c** as **a**, but for anomalies for nighttime heatwaves **b** and compound heatwaves **c**, respectively. Moisture flux is positive downwards. The shading and vector denote statistically significant at the 0.05 level by the Student's *t*-test.

## METHODS

### Datasets

Daily maximum temperature ( $T_{\max}$ ) and daily minimum temperature ( $T_{\min}$ ) for 1979–2020 are derived from the European Center for Medium-Range Weather Forecasts Reanalysis 5 (ERA5) hourly 2-meter temperature (T2m) dataset at a spatial resolution of  $2.5^\circ \times 2.5^\circ$ <sup>75</sup>. Hourly ERA5 reanalysis of other atmospheric variables, including 2-meter specific humidity, cloud cover, soil moisture, surface radiation, heat flux, and vertical integration of moisture fluxes are also used for exploring the local mechanisms associated with three types of heatwaves (i.e., daytime, nighttime, and compound heatwaves). The 2-meter specific humidity is derived from dew point temperature and pressure by applying the Python package *MetPy*. Daily precipitation is retrieved via the NOAA Climate Prediction Center (CPC) dataset

(<https://psl.noaa.gov/data/gridded/data.cpc.globalprecip.html>, available at a horizontal resolution of  $0.5^\circ \times 0.5^\circ$ ), and is interpolated onto a horizontal resolution of  $2.5^\circ \times 2.5^\circ$ , consistent with other variables.

### Definition of heatwaves on a grid-scale

We define a hot day (night) as the day when  $T_{\max}$  ( $T_{\min}$ ) exceeds its prescribed threshold<sup>76</sup>, and three or more consecutive hot days (nights) are identified as a daytime (nighttime) heatwave event<sup>10,20</sup>. So far there is no universal definition of the prescribed thresholds, and most previous studies utilized either an absolute threshold (e.g.,  $35^\circ\text{C}$ ), fixed percentile threshold, or sliding percentile threshold to select heatwave events<sup>18,46,63</sup>. However, the absolute threshold cannot represent the high spatial variability of temperatures<sup>55,77</sup>, and the fixed percentile threshold cannot be

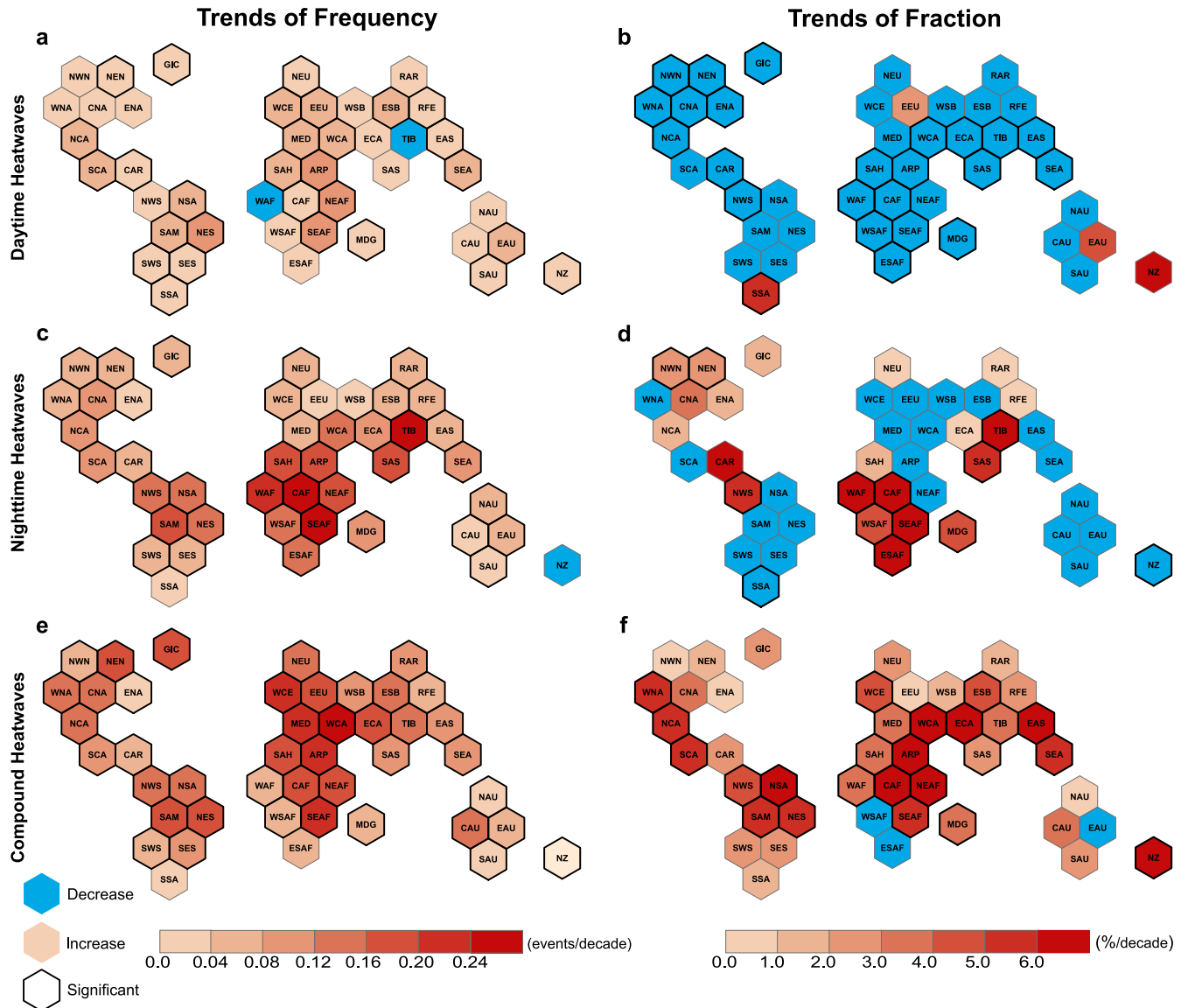


**Fig. 10 Regional trends of the frequency and fraction of different heatwaves.** **a, c, e** Spatial distribution of the long-term trends of frequency of daytime **a**, nighttime **c**, and compound heatwaves **e** during 1979–2020 over the IPCC AR6 WGI reference regions<sup>65</sup>. **b, d, f** As **a, c, e** but for fraction trends. Each hexagon corresponds to one of the IPCC AR6 WGI reference regions (see Supplementary Table 1). The trends passing the 0.05 significance level based on the mMK test are marked by a black border.

used for detecting extreme heat events in early or late summer<sup>23,76</sup>. By contrast, the sliding percentile threshold allows one to consider the possible heterogeneity of temperatures across the study region<sup>78</sup>. We thus use the 90<sup>th</sup> percentile of daily  $T_{\max}$  and  $T_{\min}$  (denoted as  $T_{\max}^{90p}$  and  $T_{\min}^{90p}$ , respectively) based on a 15-day moving window centered on each calendar day over the reference period of 1981–2010 to detect heatwave events, following previous studies<sup>26,40</sup>. In this way, the independent daytime heatwave is defined as more than three consecutive hot days without following hot nights (i.e.,  $T_{\max} \geq T_{\max}^{90p}$  and  $T_{\min} < T_{\min}^{90p}$ , see an example in Supplementary Fig. 7a). Similarly, the independent nighttime heatwave is defined as  $T_{\max} < T_{\max}^{90p}$  and  $T_{\min} \geq T_{\min}^{90p}$  (see an example in Supplementary Fig. 7b). A compound heatwave is defined as the period of three or more consecutive days when both daily  $T_{\max}$  and  $T_{\min}$  exceed their corresponding 90<sup>th</sup> percentiles (i.e.,  $T_{\max} \geq T_{\max}^{90p}$  and  $T_{\min} \geq T_{\min}^{90p}$ , see an example in Supplementary Fig. 7c). For each grid, the frequency of each type of heatwaves is defined as the total number of the events that occur at the grid during summertime

(June–August in the Northern Hemisphere and December–February in the Southern Hemisphere) of each year; the fraction of each category of heatwaves is defined as the ratio of the yearly frequency of the category to the total yearly number of all three categories. For instance, the fraction of daytime heatwaves in a year is calculated as the frequency of daytime events in the year divided by the sum of the frequencies of all three heatwave types in the same year. The determination of the summer season in the Northern and Southern Hemispheres is consistent with previous studies<sup>79,80</sup>.

#### Statistical methods

To determine the dominant patterns of different atmospheric variables associated with each heatwave type, we utilize composite analysis to investigate the local variables that may be linked with the synoptic behaviors of daytime, nighttime, and compound heatwaves. We first average hourly variables at each grid point during daytime hours (i.e., 11:00–17:00 local time) and nighttime hours (i.e., 23:00–05:00 local time) to obtain daytime and nighttime means,

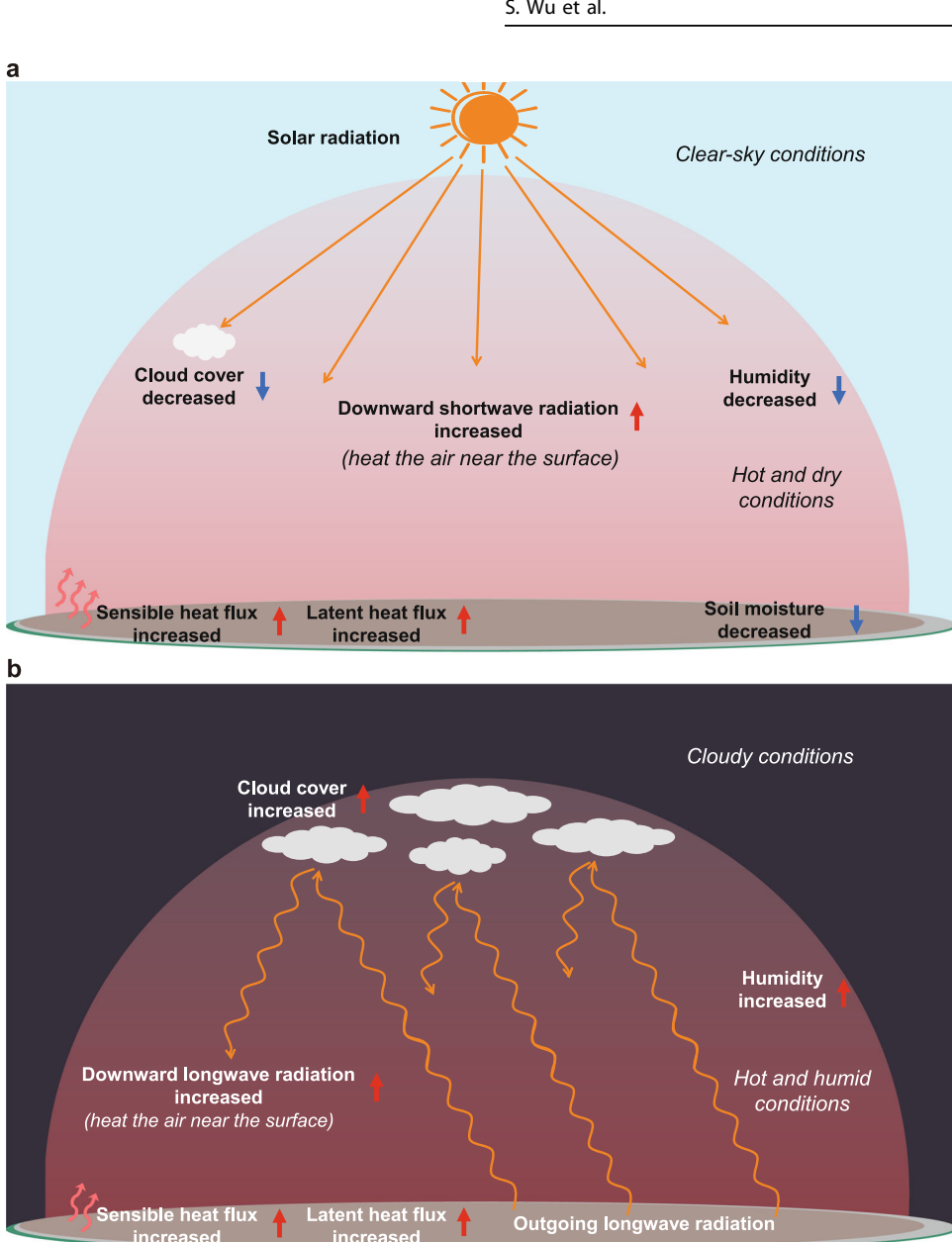


**Fig. 11 A conceptual schematic diagram for different heatwaves.** The diagram summarizes the physical processes associated with the a daytime and b nighttime heatwaves. The blue downward arrow indicates a decrease, and the red upward arrow indicates an increase.

respectively. The anomalies of daytime (nighttime) data are obtained by removing the climatological seasonal cycles from the original daytime (nighttime) series. The seasonal cycle of an atmospheric variable is calculated by averaging 30 years (i.e., the reference period of 1981–2010) and then a 31-day sliding average is applied to exclude possible short-term fluctuations<sup>81,82</sup>. Composite daytime (nighttime) anomalies for a particular type of heatwave are derived by averaging the anomalies of daytime (nighttime) data during all participating days throughout a certain type of heatwave event, and then averaging all heatwave events with equal weight. This computation is repeated for each type of heatwave events, with the significance of these anomalies evaluated by the Student's *t*-test.

#### DATA AVAILABILITY

All datasets used in this study are publicly available. The ERA5 reanalysis dataset can be downloaded from <https://cds.climate.copernicus.eu/cdsapp#!/dataset/reanalysis-era5-single-levels?tab=form>. The daily precipitation is retrieved from the NOAA

S. Wu et al.

Climate Prediction Center (CPC) dataset (<https://psl.noaa.gov/data/gridded/data.cpc.globalprecip.html>). The basemap data used to create figures is downloaded at <http://www.naturalearthdata.com/downloads/>.

#### CODE AVAILABILITY

The source codes for the analyses of this study are available from the corresponding author upon reasonable request.

Received: 11 October 2022; Accepted: 3 May 2023;  
Published online: 15 May 2023

#### REFERENCES

- Gasparini, A. & Armstrong, B. The impact of heat waves on mortality. *Epidemiology* **22**, 68–73 (2011).
- de Bonis, A., Giuliani, G., Kluser, S. & Peduzzi, P. Impacts of summer 2003 heat wave in Europe. *Environ. Alert Bull.* **2**, 1–4 (2004).

3. Dong, C., Wang, X., Ran, Y. & Nawaz, Z. Heatwaves significantly slow the vegetation growth rate on the Tibetan Plateau. *Remote Sens.* **14**, 2402 (2022).
4. Lavaysse, C. et al. Towards a monitoring system of temperature extremes in Europe. *Natural Hazards Earth Syst. Sci.* **18**, 91–104 (2018).
5. Robine, J.-M. et al. Death toll exceeded 70,000 in Europe during the summer of 2003. *Compt. Rend. Biol.* **331**, 171–178 (2008).
6. McMichael, A. J. & Lindgren, E. Climate change: present and future risks to health, and necessary responses. *J. Int. Med.* **270**, 401–413 (2011).
7. Barriopedro, D. et al. The hot summer of 2010: redrawing the temperature record map of Europe. *Science* **332**, 220–224 (2011).
8. Meehl, G. A. & Tebaldi, C. More intense, more frequent, and longer lasting heat waves in the 21st century. *Science* **305**, 994–997 (2004).
9. Luo, M. & Lau, N.-C. Increasing human-perceived heat stress risks exacerbated by urbanization in China: a comparative study based on multiple metrics. *Earth's Future*, e2020EF001848 (2021).
10. Perkins-Kirkpatrick, S. E. & Lewis, S. C. Increasing trends in regional heatwaves. *Nat. Commun.* **11**, 3357 (2020).
11. Amengual, A. et al. Projections of heat waves with high impact on human health in Europe. *Glob. Planet. Change* **119**, 71–84 (2014).
12. Cowan, T. et al. More frequent, longer, and hotter heat waves for Australia in the twenty-first century. *J. Clim.* **27**, 5851–5871 (2014).
13. Rohini, P., Rajeevan, M. & Srivastava, A. K. On the variability and increasing trends of heat waves over India. *Sci. Rep.* **6**, 26153 (2016).
14. Di Capua, G. et al. Drivers behind the summer 2010 wave train leading to Russian heatwave and Pakistan flooding. *npj Clim. Atmosph. Sci.* **4**, 55 (2021).
15. Perkins-Kirkpatrick, S. E. & Gibson, P. B. Changes in regional heatwave characteristics as a function of increasing global temperature. *Sci. Rep.* **7**, 12256 (2017).
16. You, Q. et al. A comparison of heat wave climatologies and trends in China based on multiple definitions. *Clim. Dyn.* **48**, 3975–3989 (2017).
17. You, Q. et al. Recent frontiers of climate changes in East Asia at global warming of 1.5°C and 2°C. *npj Clim. Atmosph. Sci.* **5**, 80 (2022).
18. Luo, M. et al. Observed heatwave changes in arid northwest China: physical mechanism and long-term trend. *Atmosph. Res.* **242**, 105009 (2020).
19. Ullah, I. et al. Projected changes in socioeconomic exposure to heatwaves in South Asia under changing climate. *Earth's Future* **10**, e2021EF002240 (2022).
20. Perkins-Kirkpatrick, S. E. & Alexander, L. On the measurement of heat waves. *J. Clim.* **26**, 4500–4517 (2013).
21. Chen, R. & Lu, R. Dry tropical nights and wet extreme heat in Beijing: a typical configurations between high temperature and humidity. *Monthly Weather Rev.* **142**, 1792–1802 (2014).
22. Li, Y., Ding, Y. & Li, W. Observed trends in various aspects of compound heat waves across China from 1961 to 2015. *J. Meteorol. Res.* **31**, 455–467 (2017).
23. Wang, J. et al. Anthropogenically-driven increases in the risks of summertime compound hot extremes. *Nat. Commun.* **11**, 528 (2020).
24. Wang, J., Feng, J., Yan, Z. & Chen, Y. Future risks of unprecedented compound heat waves over three vast urban agglomerations in China. *Earth's Future* **8**, e2020EF001716 (2020).
25. Karl, T. R. & Knight, R. W. The 1995 Chicago heat wave: how likely is a recurrence? *Bull. Am. Meteorol. Soc.* **78**, 1107–1120 (1997).
26. Luo, M., Lau, N.-C. & Liu, Z. Different mechanisms for daytime, nighttime, and compound heatwaves in Southern China. *Weather Clim. Extremes* **36**, 100449 (2022).
27. Yoon, D. et al. Impacts of synoptic and local factors on heat wave events over southeastern region of Korea in 2015. *J. Geophys. Res. Atmosph.* **123**, 12081–012096 (2018).
28. Fischer, E. M., Seneviratne, S. I., Lüthi, D. & Schär, C. Contribution of land-atmosphere coupling to recent European summer heat waves. *Geophys. Res. Lett.* **34**, L06707 (2007).
29. Chang, F.-C. & Wallace, J. M. Meteorological conditions during heat waves and droughts in the United States Great Plains. *Monthly Weather Rev.* **115**, 1253–1269 (1987).
30. Wu, Z. et al. Heat wave frequency variability over North America: two distinct leading modes. *J. Geophys. Res. Atmosph.* **117**, D02102 (2012).
31. Luo, M. & Lau, N.-C. Heat waves in southern China: synoptic behavior, long-term change and urbanization effects. *J. Clim.* **30**, 703–720 (2017).
32. Deng, K. et al. An intensified mode of variability modulating the summer heat waves in Eastern Europe and Northern China. *Geophys. Res. Lett.* **45**, 11361–311369 (2018).
33. Harpaz, T., Ziv, B., Saaroni, H. & Beja, E. Extreme summer temperatures in the East Mediterranean—dynamical analysis. *Int. J. Climatol.* **34**, 849–862 (2014).
34. Ziv, B., Saaroni, H. & Alpert, P. The factors governing the summer regime of the eastern Mediterranean. *Int. J. Climatol.* **24**, 1859–1871 (2004).
35. Teng, H. et al. Probability of US heat waves affected by a subseasonal planetary wave pattern. *Nat. Geosci.* **6**, 1056–1061 (2013).
36. Coumou, D., Lehmann, J. & Beckmann, J. The weakening summer circulation in the Northern Hemisphere mid-latitudes. *Science* **348**, 324–327 (2015).
37. Schubert, S., Wang, H. & Suarez, M. Warm season subseasonal variability and climate extremes in the Northern Hemisphere: the role of stationary Rossby waves. *J. Clim.* **24**, 4773–4792 (2011).
38. Luo, M. et al. An observational investigation of spatiotemporally contiguous heatwaves in China from a 3D perspective. *Geophys. Res. Lett.* **49**, e2022GL097714 (2022).
39. Gershunov, A., Cayan, D. R. & Iacobellis, S. F. The great 2006 heat wave over California and Nevada: signal of an increasing trend. *J. Clim.* **22**, 6181–6203 (2009).
40. Thomas, N. et al. Mechanisms associated with daytime and nighttime heat waves over the contiguous United States. *J. Appl. Meteorol. Climatol.* **59**, 1865–1882 (2020).
41. Bumbaco, K. A., Dello, K. D. & Bond, N. A. History of Pacific Northwest heat waves:synoptic pattern and trends. *J. Appl. Meteorol. Climatol.* **52**, 1618–1631 (2013).
42. Hong, J.-S., Yeh, S.-W. & Seo, K.-H. Diagnosing physical mechanisms leading to pure heat waves versus pure tropical nights over the Korean Peninsula. *J. Geophys. Res. Atmosph.* **123**, 7149–7160 (2018).
43. Li, Y., Ding, Y. & Liu, Y. Mechanisms for regional compound hot extremes in the mid-lower reaches of the Yangtze River. *Int. J. Climatol.* **41**, 1292–1304 (2020).
44. Davy, R. et al. Diurnal asymmetry to the observed global warming. *Int. J. Climatol.* **37**, 79–93 (2017).
45. Vose, R. S., Easterling, D. R., & Gleason, B. Maximum and minimum temperature trends for the globe: an update through 2004. *Geophys. Res. Lett.* **32**, L23822 (2005).
46. Black, E. et al. Factors contributing to the summer 2003 European heatwave. *Weather* **59**, 217–223 (2004).
47. Marengo, J. A. et al. The heat wave of October 2020 in central South America. *Int. J. Climatol.* **42**, 2281–2298 (2022).
48. Chen, R. & Lu, R. Large-scale circulation anomalies associated with ‘tropical night’ weather in Beijing, China. *Int. J. Climatol.* **34**, 1980–1989 (2014).
49. Philipona, R., Dür, B., Ohmura, A. & Ruckstuhl, C. Anthropogenic greenhouse forcing and strong water vapor feedback increase temperature in Europe. *Geophys. Res. Lett.* **32**, L19809 (2005).
50. Fischer, E. M. et al. Soil moisture–atmosphere interactions during the 2003 European summer heat wave. *J. Clim.* **20**, 5081–5099 (2007).
51. Ford, T. W. & Schoof, J. T. Characterizing extreme and oppressive heat waves in Illinois. *J. Geophys. Res. Atmosph.* **122**, 682–698 (2017).
52. Dirmeyer, P. A. et al. Land-atmosphere interactions exacerbated the drought and heatwave over northern Europe during summer 2018. *AGU Adv.* **2**, e2020AV000283 (2021).
53. Zhang, Y. et al. Aircraft observed diurnal variations of the planetary boundary layer under heat waves. *Atmosph. Res.* **235**, 104801 (2020).
54. Qiu, G. Y. et al. Water use efficiency and evapotranspiration of winter wheat and its response to irrigation regime in the north China plain. *Agric. Forest Meteorol.* **148**, 1848–1859 (2008).
55. Ullah, S. et al. Daytime and nighttime heat wave characteristics based on multiple indices over the China–Pakistan economic corridor. *Clim. Dyn.* **53**, 6329–6349 (2019).
56. Hartmann D. L. *Glob. Phys. Climatol.* Newnes (2016).
57. Koster, R., Fekete, B., Huffman, G. & Stackhouse Jr, P. Revisiting a hydrological analysis framework with International Satellite Land Surface Climatology Project Initiative 2 rainfall, net radiation, and runoff fields. *J. Geophys. Res.* **111**, D22S05 (2006).
58. Tomczyk, A. M., Bednorz, E. & Pórolnyczak, M. The occurrence of heat waves in Europe and their circulation conditions. *Geografie* **124**, 1–17 (2019).
59. Lee, W.-S. & Lee, M.-I. Interannual variability of heat waves in South Korea and their connection with large-scale atmospheric circulation patterns. *Int. J. Climatol.* **36**, 4815–4830 (2016).
60. Ruffault, J. et al. Extreme wildfire events are linked to global-change-type droughts in the northern Mediterranean. *Natural Hazards Earth Syst. Sci.* **18**, 847–856 (2018).
61. Coffel, E. D. et al. Future hot and dry years worsen nile basin water scarcity despite projected precipitation increases. *Earth's Future* **7**, 967–977 (2019).
62. Feng, S., Hao, Z., Zhang, X. & Hao, F. Changes in climate-crop yield relationships affect risks of crop yield reduction. *Agric. Forest Meteorol.* **304–305**, 108401 (2021).
63. Zhai, P. & Pan, X. Trends in temperature extremes during 1951–1999 in China. *Geophys. Res. Lett.* **30**, 1913 (2003).
64. Karl, T. R. et al. Global warming: evidence for asymmetric diurnal temperature change. *Geophys. Res. Lett.* **18**, 2253–2256 (1991).
65. Iturbide, M. et al. An update of IPCC climate reference regions for subcontinental analysis of climate model data: definition and aggregated datasets. *Earth Syst. Sci. Data* **12**, 2959–2970 (2020).

and Technology) for Young and Middle-aged Teachers in Fujian Province 2021, Education Department of Fujian Province (No. Kla21005A). The appointment of M.L. at Sun Yat-sen University is partially supported by the Pearl River Talent Recruitment Program of Guangdong Province (No. 2017GC010634). The appointment of Z.L. is supported by the Institute for Basic Science (IBS), Republic of Korea, under No. IBS-R028-D1.

## AUTHOR CONTRIBUTIONS

M.L. designed the research. S.W. carried out the analyses and wrote the first draft of the paper. All authors worked together on the interpretation of the results and commented on the paper.

## COMPETING INTERESTS

The authors declare no competing interests.

## ADDITIONAL INFORMATION

**Supplementary information** The online version contains supplementary material available at <https://doi.org/10.1038/s41612-023-00365-8>.

**Correspondence** and requests for materials should be addressed to Ming Luo.

**Reprints and permission information** is available at <http://www.nature.com/reprints>

**Publisher's note** Springer Nature remains neutral with regard to jurisdictional claims in published maps and institutional affiliations.



**Open Access** This article is licensed under a Creative Commons Attribution 4.0 International License, which permits use, sharing, adaptation, distribution and reproduction in any medium or format, as long as you give appropriate credit to the original author(s) and the source, provide a link to the Creative Commons license, and indicate if changes were made. The images or other third party material in this article are included in the article's Creative Commons license, unless indicated otherwise in a credit line to the material. If material is not included in the article's Creative Commons license and your intended use is not permitted by statutory regulation or exceeds the permitted use, you will need to obtain permission directly from the copyright holder. To view a copy of this license, visit <http://creativecommons.org/licenses/by/4.0/>.

© The Author(s) 2023

66. Ha, K.-J. & Yun, K.-S. Climate change effects on tropical night days in Seoul, Korea. *Theor. Appl. Climatol.* **109**, 191–203 (2012).
67. Ding, T., Qian, W. & Yan, Z. Changes in hot days and heat waves in China during 1961–2007. *Int. J. Climatol.* **30**, 1452–1462 (2010).
68. Freychet, N., Tett, S., Wang, J. & Hegerl, G. Summer heat waves over Eastern China: dynamical processes and trend attribution. *Environ. Res. Lett.* **12**, 024015 (2017).
69. Wang, P. et al. Heat waves in China: definitions, leading patterns, and connections to large-scale atmospheric circulation and SSTs. *J. Geophys. Res. Atmosph.* **122**, 10679–610699 (2017).
70. Budikova, D., Ford, T. W. & Ballinger, T. J. United States heat wave frequency and Arctic ocean marginal sea ice variability. *J. Geophys. Res. Atmosph.* **124**, 6247–6264 (2019).
71. Schaller, N. et al. Influence of blocking on Northern European and Western Russian heatwaves in large climate model ensembles. *Environ. Res. Lett.* **13**, 054015 (2018).
72. Tang, Q., Zhang, X. & Francis, J. A. Extreme summer weather in northern mid-latitudes linked to a vanishing cryosphere. *Nat. Clim. Change* **4**, 45–50 (2014).
73. Gao, T., Luo, M., Lau, N. C. & Chan, T. Spatially distinct effects of two El Niño types on summer heat extremes in China. *Geophys. Res. Lett.* **47**, e2020GL086982 (2020).
74. Luo, M. & Lau, N.-C. Amplifying effect of ENSO on heat waves in China. *Clim. Dyn.* **52**, 3277–3289 (2019).
75. Hersbach, H. et al. The ERA5 global reanalysis. *Quart. J. R. Meteorol. Soc.* **146**, 1999–2049 (2020).
76. Della-Marta, P., Haylock, M., Luterbacher, J. & Wanner, H. Doubled length of western European summer heat waves since 1880. *J. Geophys. Res. Atmosph.* **112**, D15103 (2007).
77. Smith, T. T., Zaitchik, B. F. & Gohlke, J. M. Heat waves in the United States: definitions, patterns and trends. *Clim. Change* **118**, 811–825 (2013).
78. Zhang, X., Hegerl, G., Zwiers, F. W. & Kenyon, J. Avoiding inhomogeneity in percentile-based indices of temperature extremes. *J. Clim.* **18**, 1641–1651 (2005).
79. Bathiany, S., Dakos, V., Scheffer, M. & Lenton, T. M. Climate models predict increasing temperature variability in poor countries. *Sci. Adv.* **4**, eaar5809 (2018).
80. Vogt, L., Burger, F. A., Griffies, S. M. & Frölicher, T. L. Local drivers of marine heatwaves: a global analysis with an Earth system model. *Front. Clim.* **4**, 847995 (2022).
81. Lau, N.-C. & Nath, M. Model simulation and projection of European heat waves in present-day and future climates. *J. Clim.* **27**, 3713–3730 (2014).
82. Luo, M. & Lau, N.-C. Synoptic characteristics, atmospheric controls, and long-term changes of heat waves over the Indochina Peninsula. *Clim. Dyn.* **51**, 2707–2723 (2018).
83. Hamed, K. H. & Rao, R. A. A modified Mann-Kendall trend test for autocorrelated data. *J. Hydrol.* **204**, 182–196 (1998).

## ACKNOWLEDGEMENTS

This work is supported by the National Natural Science Foundation of China (Nos. 41871029 and 42207271), and Educational and Scientific Research Projects (Science